Chapter 5 Cluster spin-glass transition in $Ca(Fe_{1/2}Nb_{1/2})O_3$

5.1. Introduction

As discussed in chapter I, complex perovskites with a general formula $A(B^{'}B^{''})O_3$, where A is an alkaline metal ion Pb^{2+}, Ba^{2+}, Sr^{2+}, Ca^{2+}, $B^{'}$ is a transition metal ion Fe^{3+}, Ni^{2+}, Co^{2+} with partially filled 3d orbital and $B^{''}$ is a ferro-active ion like Nb^{5+}, Ta^{5+}, W^{6+} with $4d^0/5d^0$ configuration were synthesized by Russian scientist to exhibit magnetoelectric multiferroic characteristics [147,183,184]. These compounds have both site as well as charge disorder at the B-site occupied by $B^{'}$ and $B^{''}$ cations randomly. Despite the presence of magnetic and ferro-active ions at the B-site in 1:1 proportion, only the Pb^{2+} based compounds, like $Pb(Fe_{1/2}Nb_{1/2})O_3$ (PFN) [171,172], $Pb(Fe_{1/2}Ta_{1/2})O_3$ (PFT) [174], and $Pb(Fe_{2/3}W_{1/3})O_3$ (PFW) [191] exhibit long range ordered (LRO) antiferromagnetic (AFM) and ferroelectric (FE)/relaxor ferroelectric (RFE) transitions at T_N~150K, 150-180K and 350K and T_c at 385K, 240K and 150K, respectively. The Pb^{2+} free compounds do not exhibit either LRO AFM or FE/RFE states [176–178]. However, all these complex perovskites exhibit a spin glass (SG) like transition at low temperature. The SG freezing temperature T_f for Pb^{2+} based and Pb^{2+} free compounds are around 10 and 25K, respectively [171,172,176–178]. While the SG transition has been properly investigated using macroscopic (DC and AC susceptibilities (χ_{DC}, $\chi(\omega, T)$) and microscopic (neutron, Mössbauer, µSR) and local probes like (NMR, EPR, EXAFS and PDF) techniques only in Pb^{2+} based compounds [171,172], especially PFN, the so-called evidence for SG transition in Pb^{2+} free complex perovskites has been limited to the observation of irreversibility of the field cooled (FC) and zero-field cooled (ZFC) magnetization M(T). Since such an irreversibility occurs in superparamagnetic systems [198] also, there is a need to test the existence of SG transition using other criterion also discussed in chapter III in relation to disordered $BiFeO_3$ system.

Despite the extensive literature, the origin of the SG phase in the well-known multiferroic PFN is still controversial as discussed in chapter I. Two different models have been proposed in the literature [171,172]. According to one of these models based on macroscopic measurements, the LRO AFM phase of PFN results from the infinite percolative clusters of Fe^{3+} spins while the glassy phase is a consequence of the freezing of the finite size isolated clusters with uncompensated Fe^{3+} spin [171]. This model implies that the SG and LRO AFM phases occur on two separate sublattices. In the second model, which is based on microscopic measurements (neutron and Mössbauer techniques), on the other hand, the SG phase is argued to result from the LRO AFM sub-lattice system itself due to freezing of the transverse component of the spins in a glassy manner [172]. Since the controversy in this compound is due to the complications introduced by the coexistence of SG and LRO AFM phases, the Pb-free compounds can provide an ideal platform to resolve this controversy as they do not exhibit any LRO AFM transition. Taking this objective in mind, we present in this chapter results of a comprehensive study of the spin-glass state of $Ca(Fe_{1/2}Nb_{1/2})O_3$ using both macroscopic and microscopic measurements.

5.2. Sample preparation:

Polycrystalline $Ca(Fe_{1/2}Nb_{1/2})O_3$ (CFN) was synthesized by standard solid-state route using high purity carbonate ($CaCO_3$) and oxides (Fe_2O_3, Nb_2O_5) supplied by Sigma Aldrich. The stoichiometric powders were first mixed in an agate mortar and pestle for 2 hours. The mixture was then ball milled (Retsch GmbH, Germany) for 6 hours in the presence of acetone as the mixing media in a zirconia jar using zirconia balls. After evaporation of the acetone, the mixed powder was calcined at 1423 K for 10 hours in an open alumina crucible. The calcined powder was crushed into fine powder and again ball milled for 4 hours, dried and then pressed into pellets (diameter 12mm, thickness ~1mm) using cylindrical steel die of 12mm diameter and a uniaxial hydraulic press at an optimized load of 70 kN. A 2% polyvinyl alcohol (PVA) aqueous solution was used as a binder for making the green pellets. After binder burn-off at 773 K for 10 hours, sintering of the green pellets was carried out at 1523 K for 3 hours in open air. Powders obtained after crushing the sintered pellets were annealed at 773K for 10 hours to remove any strains developed during crushing. The annealed powders were used in all the measurements.

5.3. Characterizations:

Microstructure of the $Ca(Fe_{1/2}Nb_{1/2})O_3$ pellet was obtained using a Carl-Zeiss Scanning Electron Microscope (SEM), model no. EVO 18. The chemical compositions were checked by Energy Dispersive X-ray spectroscopy (EDX) attachment (Oxford, model no. 51-ADD0048) in the above-mentioned SEM and Electron Probe Micro Analyzer (EPMA) using CAMECA SXFive instrument. The sintered pellet was coated with conducting gold using sputter coater (Royal life Sciences, model no. DSR1) under vacuum before taking the SEM images. For EPMA analysis, the sintered pellet was coated with 20 nm thin layer of carbon using LEICA-EM ACE200 instrument. Natural silicate mineral andardite as internal standard used to verify positions of crystals (SP1-PET, SP2-LiF and SP4-LPC0) with respect to corresponding wavelenght dispersive spectrometers in CAMECA SX-Five instrument. The following X-ray lines were used in the analyses: O-$K\alpha$, Ca-$K\alpha$, Fe-$K\alpha$, and Nb-$L\alpha$. Routine calibration, acquisition, quantification and data processing were carried out using SxSAB version 6.1 and SX-Results softwares of CAMECA.

X-ray powder diffraction (XRD) measurement was carried out using an 18-kW Cu rotating anode powder diffractometer (Rigaku, model no. RINT 2500/PC series) operating in the Bragg-Brentano geometry and fitted with a curved crystal monochromator in the diffraction beam. The data were collected in the 2θ range 20 to 120° at a step of 0.02 degrees.

High-resolution synchrotron x-ray powder diffraction (SXRD) data at room temperature was also collected at P02.1 beamline of PETRA III, Hamburg, Germany, at a wavelength of 0.2079Å (~60keV) to determine the phase purity and crystal structure. The powder sample was filled in a Kapton capillary of 0.6mm diameter and exposed to the incident beam of cross section of 0.5 mm × 0.5 mm for 10 s. Two-dimensional (2D) XRD pattern was recorded using a Perkin Elmer 1621 Detector (2048 pixels × 2048 pixels, 200µm × 200µm pixel size). The sample to detector distance was set to 1310 mm. The standard LaB_6 was used to calibrate the sample to detector distance. The 2D XRD pattern was integrated using the FIT2D software.

High-resolution neutron powder diffraction (NPD) patterns were collected in the temperature range 5-300K using structure powder diffractometer SPODI at FRM-II research reactor in Garching, Germany . The incident neutron wavelength was 1.5482Å as obtained from germanium (551) reflection of vertically focussed monochromator at a take-off angle of 155°. Approximately 12g powder sample was kept in a cylindrical vanadium (V) can of diameter 4mm which was cooled to different temperatures using close cycle helium refrigerator. The data were recorded at a step of 0.05° in the 2θ range from 5 to 150°. The nuclear structure was refined by Rietveld technique using software package “FULLPROF” [253].

DC magnetization M (T, H) and AC susceptibility (χ (ω, T)) measurements were carried out on a superconducting quantum interference device (SQUID) based magnetometer (Quantum Design, MPMS-3).

5.4. Results and discussion:

5.4.1 Microstructure and chemical composition analysis:

The scanning electron microscopic image of the microstructure of CFN is shown in Fig. 5.1(a). The average grain size calculated by linear intercept method is found to be approximately 1.4 μm. The EDX spectra of CFN are shown on the right panel (see Fig. 5.1(b)). The chemical composition of the sample was determined through a quantitative analysis of the EDX spectra. The average composition of the ceramic sample was confirmed through EPMA analysis also as its results are more accurate. The results of EDX and EPMA are compared in Table 5.1 which confirms that the composition of the samples corresponds to the nominal composition within the standard deviation.

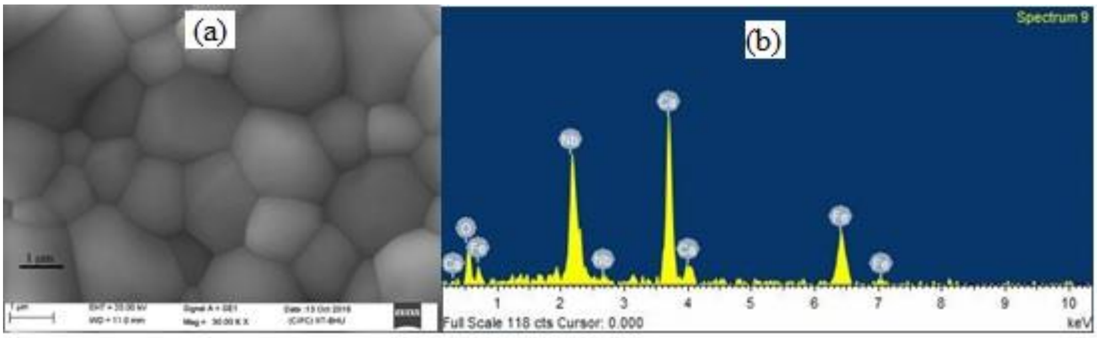

Figure 5.1: Scanning electron micrograph and EDX spectra of $Ca(Fe_{1/2}Nb_{1/2})O_3$.

Table 5.1: Quantification of $Ca(Fe_{1/2}Nb_{1/2})O_3$ by EDX and EPMA analysis

Average chemical composition in weight %			
Element	Expected	Observed by	
		EDX	EPMA
Ca	24.7	24.1 ± 1.0	23.8 ± 0.5
Fe	17.2	17.3 ± 1.0	16.7 ± 0.2
Nb	28.6	29.8 ± 0.5	28.9 ± 0.8
O	29.5	28.7 ± 0.8	28.3 ± 0.5

5.4.2 Phase purity and crystal structure:

The x-ray powder diffraction (XRD) pattern of $Ca(Fe_{1/2}Nb_{1/2})O_3$ (CFN) along with those of calcium carbonate ($CaCO_3$), iron oxide (Fe_2O_3) and niobium oxide (Nb_2O_5) are shown in Fig. 5.2. All the peaks in the diffraction patterns of CFN could be indexed with an orthorhombic unit cell. The absence of the strongest peaks of the $CaCO_3$, Fe_2O_3 and Nb_2O_5 in the CFN pattern confirms that the powder does not contains any impurity phases. The very small peaks, marked with arrows in the diffraction pattern of CFN, are not due to any unreacted ingradients or some unwanted phases but are the superlattice reflection arising from unit cell doubling. The phase purity was further confirmed by the high-resolution synchrotron x-ray powder diffraction (SXRD) data shown in Fig. 5.3. It is evident from the figure that all the peaks in the SXRD patterns of the sintered powder of CFN could be indexed with the orthorhombic phase and no trace of any impurity phase is observed.

The superlattice reflections can arise due to cation ordering at the B-site of the perovskite structure. The differences in the charges that occupy the same site in the unit cell can promote the ordering of the cations to minimize the electrostatic energy [19,151]. Further, the significant size difference of the cations occupying the same site in the unit cell can also promote the cations ordering to minimize the elastic strain energy [151]. The most common ordering at the B-site in these complex perovskites compound is the (111) or rock-salt ordering that leads to a doubling of the unit cell in every direction [147]. The ordering of the cations leads to change in the space group symmetry also [201,202]. In case of CFN, the significant charge difference in the B-site of Fe^{3+} and Nb^{5+} may promote the ordering of the cations to minimize the electrostatic energy. Since the size difference of the Fe^{3+} = 0.645 Å, and Nb^{5+} = 0.64 Å ions at the B-site is small (0.005Å), it may not promote ordering of the cations. Another common source of unit cell doubling in

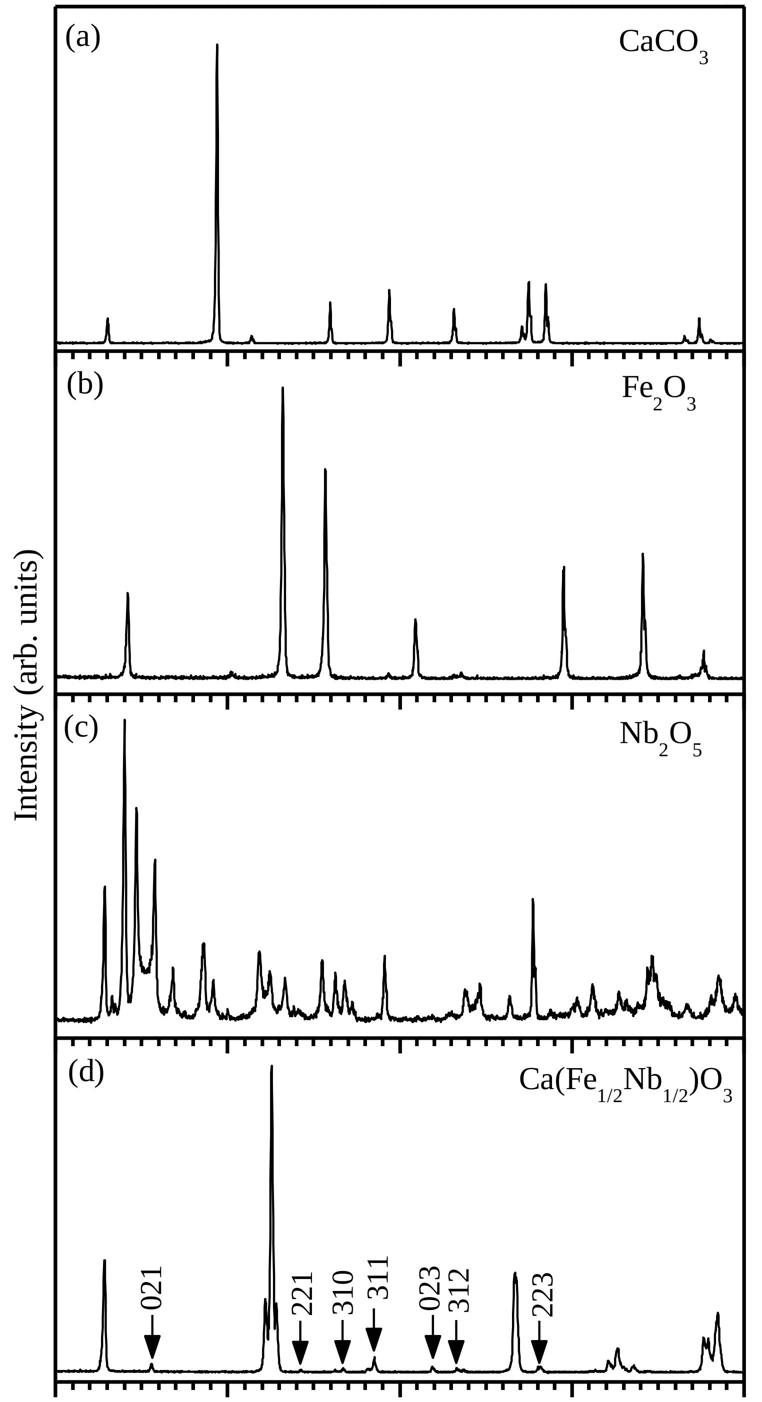

Figure 5.2: X-ray powder diffraction patterns of (a) $CaCO_3$ (b) Fe_2O_3 (c) Nb_2O_5 and (d) $Ca(Fe_{1/2}Nb_{1/2})O_3$. The positions of superlattice reflections for the orthorhombic structure with the Pbnm space group, are marked by arrows. All the indices are written with respect to the double cubic perovskite cell.

complex perovskites is the tilting of the BO_6 octahedra. According to Glazer, the tilts can be described by three components about the three tetrad axes namely a, b, c of the elementary perovskite unit cell. Each tilt about a given axis forces tilt of opposite sense about the other two tetrad axes leading to the doubling of the corresponding unit cell parameters. In addition, the octahedra along the tilt axis in the neighbouring unit cells may be tilted in-phase or anti-phase. For anti-phase tilting, the unit cell will be doubled along the tilt axis also. In Glazer's notation [204], aaa means equal tilts about all the three axes and abc means three unequal tilts. Thus aac means equal tilt about [100] and [010] but unequal tilt about [001]. The in-phase tilt is denoted by '+' sign as superscript while the anti-phase tilt is denoted by '-' sign as superscript. The absence of tilt is denoted by '0' in the superscript. Thus $a^0a^0c^-$ means that the structure has antiphase tilting about the pseudo-cubic c axis and no tilt about the a and b axes. Thus, the cation ordering, in-phase and anti-phase octahedral tilting may give rise to a set of superlattice reflections which may be indexed with respect to a doubled perovskite cell. The fundamental perovskite reflections acquire Miller indices (hkl) which are all even (eee-type) integers while the reflections that arise from either B-site cation ordering or anti-phase octahedral tilting have Miller indices that corresponds to h, k and l being all odd (ooo-type). The anti-phase octahedral tilt is known to be linked with phonon instability at the R (q =½ ½ ½) point of the Brillouin zone of the elementary perovskite unit cell, as was first confirmed in $SrTiO_3$ [5]. The superlattice reflections that arise from the in-phase tilting of the octahedra have two odd integer indices and one even integer (ooe-type) and is known to be associated with M (q = ½ ½ 0) point phonon instability [14]. Further, the antiparallel A-site cation displacements also results in the unit cell doubling and leads to superlattice reflections of the even-even-odd (eeo-type) observed in the orthorhombic $CaTiO_3$ [14]. Jahn-Teller distortion can also distort the shape of the octahedra which may lead to doubling of the unit cell and hence produce superlattice reflections [14] but the complex perovskite under present discussion do not have a John-Teller active ion at the B-site. In CFN, we observe three types of superlattice reflections having indices odd-odd-odd and odd-odd-even and even-even-odd with respect to the doubled perovskite cell. The presence of odd-odd-odd and odd-odd-even types of superlattice reflection in CFN confirms the anti-phase and in-phase tilts in CFN.

The room temperature crystal structure of CFN is controversial as both orthorhombic (disordered) Pbnm space group based on $a^-a^-c^+$ tilt system with B-site cation ordering [176,199,200] and monoclinic (ordered) $P2_1/n$ space group [200–202] with $a^-a^-c^+$ tilt as well as B-site cation ordering have been proposed in the literature [201,202]. In order to resolve the existing controversy about the room temperature crystal structure of CFN, we have performed the Rietveld refinement using SXRD pattern using space group symmetries $P2_1/n$ and Pbnm corresponding to ordered monoclinic and B-site disordered orthorhombic structures. The asymmetric unit of the orthorhombic structure of CFN consists of Ca^{2+}, Fe^{3+}/Nb^{5+}, O^{2-}_{I} and O^{2-}_{II} at (x, y, 1/4), (1/2, 0, 0), (x, y, 1/4) and (x, y, z) corresponding to the Wyckoff sites 4c, 4b, 4c and 8d, respectively. The asymmetric unit of monoclinic phase, consists of Ca^{2+} at the 4e sites and x, y, z general positions, Fe^{3+} at 2d site with 1/2, 0, 0 special position, Nb^{5+} at 2c site with 0, 1/2, 0 special position, and the three oxygen (O_1 O_2 and O_3) at 4e sites with x, y, z general positions. In the Rietveld refinement, the background and peak shape were modelled with linear interpolation and pseudo-Voigt function, respectively while the occupancy was fixed at the nominal composition. Zero correction, scale factor, background, lattice parameters, half width parameters (u, v, w), positional coordinates and thermal parameters were varied during the refinement which converged after a few cycles. Figs. 5.3(a) and (b) depict the comparison of observed and calculated SXRD profiles obtained by Rietveld refinement using monoclinic ($P2_1/n$) and orthorhombic (Pbnm) space group symmetries, respectively. It is evident from the figures that the observed (filled-circles) and calculated (continuous line) profiles show excellent fit for the orthorhombic phase with Pbnm space group as can be seen from the nearly flat difference profile (bottom line) in the same figure. The superlattice reflections expected from the cation ordering as well as octahedral tilt for the monoclinic $P2_1/n$ space group, on the otherhand, are not observed (see the reflections marked with arrows in the insets of Fig. 5.3(a)). Thus, rules out the chemical ordering in $Ca(Fe_{1/2}Nb_{1/2})O_3$. The Rietveld refinement using SXRD data thus confirms that CFN belongs to orthorhombic phase in the Pbnm space group in agreement with the previous reports [176,199,200] and rejects the monoclinic $P2_1/n$ space group proposed by other workers [200–202]. This was possible simply because of the use of high resolution SXRD data in the present work which revealed very weak superlattice reflections, not observable unambiguously in the laboratory source data used by previous workers [200–202].

The refined structural parameters using Pbnm space group for CFN are given in Tables 5.2. The unit cell parameters, positional coordinate and thermal parameters are in good agreement with those reported in literature [176,199,200]. Thus, CFN belongs to the $a^-a^-c^+$ tilt system in Glazer's notation with orthorhombic crystal structure in the Pbnm space group. Fig. 5.3(c) depicts the orthorhombic crystal structure of CFN along with the tilted oxygen octahedra. After setting the controversies about the structure and space group symmetry of CFN at room temperature, we now proceed to analyse the low temperature magnetic transition in CFN.

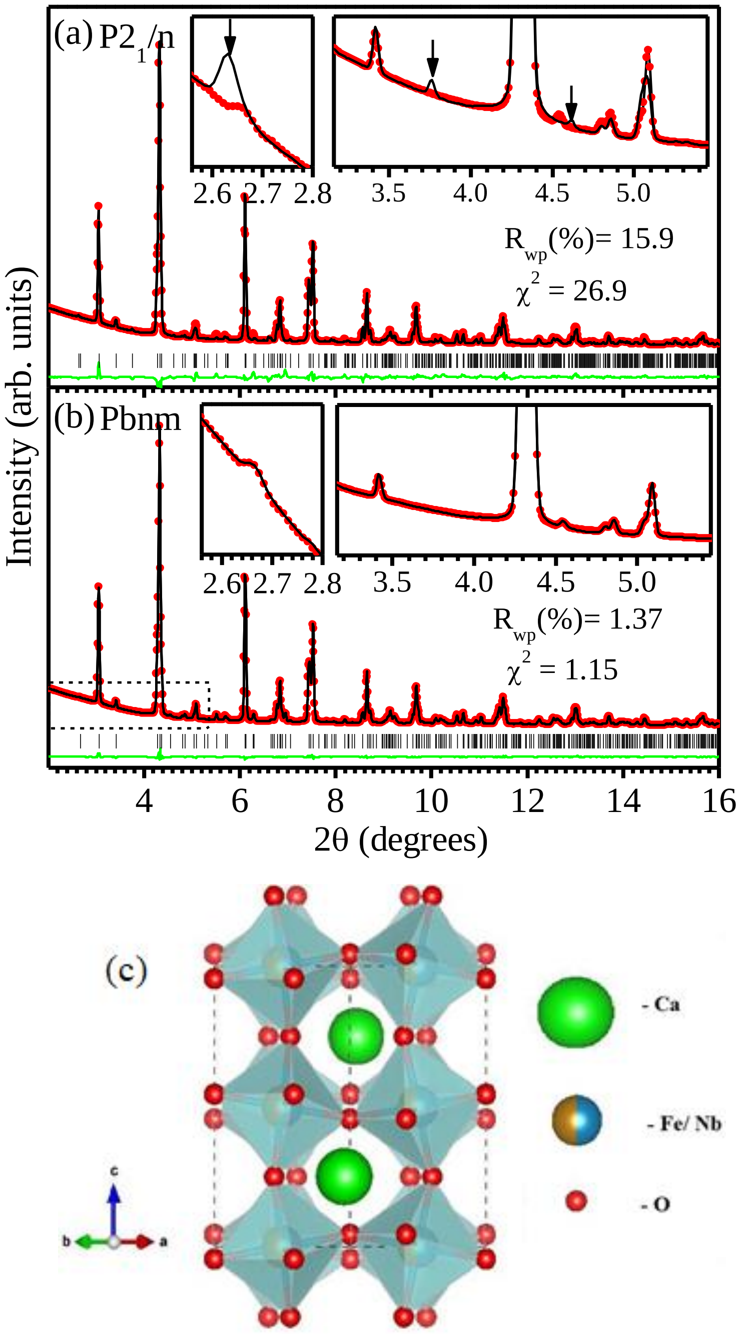

Figure 5.3: Observed (red dots), calculated (black continuous line) and difference (green continuous line) profiles obtained by Rietveld refinement using synchrotron x-ray data of Ca(Fe$_{1/2}$Nb$_{1/2}$)O$_3$ at room temperature using (a) monoclinic P2$_1$/n (b) orthorhombic Pbnm space groups. Vertical tick marks above the difference profile represent the Bragg peak positions. Arrow marked the expected positions of superlattice peak at 2.63, 3.75 and 4.62 degree for the monoclinic phase. The absence of these peaks rules out the monoclinic structure. (c) depicts the crystal structure of Ca(Fe$_{1/2}$Nb$_{1/2}$)O$_3$ along with tilted octahedra.

Table 5.2: Structural parameters obtained from the Rietveld analysis of the SXRD pattern of $Ca(Fe_{1/2}Nb_{1/2})O_3$ using orthorhombic Pbnm space group.

Atoms	x	y	z	B (Å^2)
Ca^{2+}	0.0083 (5)	0.0439 (2)	¼	1.01 (2)
Fe^{3+}/Nb^{5+}	½	0	0	0.89 (9)
$O^{2-}{}_1$	0.9170 (7)	0.4471 (6)	¼	1.02 (7)
$O^{2-}{}_2$	0.2953 (5)	0.2916 (4)	0.0425 (4)	0.77 (5)
A_o= 5.4480(1) Å, B_o = 5.5499 (1) Å, C_o = 7.7573 (2) Å: α = β = γ= 90°				

5.4.3 Evidence for history dependent irreversibility in DC magnetization studies:

The temperature dependence of dc magnetization M(T) of CFN measured during warming under a magnetic field of 100 Oe after zero-field cooling (ZFC) of the sample shows a peak at T_f ~25 K (see Fig. 5.4) in agreement with previous reports on CFN [56]. The disordered complex perovskites like $Sr(Fe_{1/2}Nb_{1/2})O_3$ (SFN), $Ba(Fe_{1/2}Nb_{1/2})O_3$ (BFN), $Ca(Fe_{1/2}Ta_{1/2})O_3$ (CFT), $Sr(Fe_{1/2}Ta_{1/2})O_3$ (SFT), and $Ba(Fe_{1/2}Ta_{1/2})O_3$ (BFT) also show T_f around 25K [176–178]. Pb-based disordered complex perovskites, like PFN, $Pb(Fe_{1/2}Ta_{1/2})O_3$ (PFT), $Pb(Fe_{2/3}W_{1/3})O_3$ (PFW), on the otherhand, show lower T_f ~10K [171,172,174,175,191]. As discussed in the next chapter, the Curie-Weiss temperature (θ_{CW}) obtained from high temperature DC susceptibility (χ_{dc}) data is –(113.7±0.8)K. Thus large negative value of θ_{CW} reveals predominant antiferromagnetic interactions in CFN but there is no signature of any AFM transition in the ZFC M(T) plot of CFN in marked contrast to PFN and PFT which show a small anomaly at T_N ~150K [171,172,174,175]. The ZFC and FC M(T) plots at 100 Oe, shown in Fig. 5.4 reveal bifurcation of the two curves at the irreversibility temperature T_{irr} ~27K, which is a characteristic of SG freezing [24,41–43]. However, such a bifurcation is known to occur in an ensemble of non-interacting SPM spin clusters also due to the onset of blocking

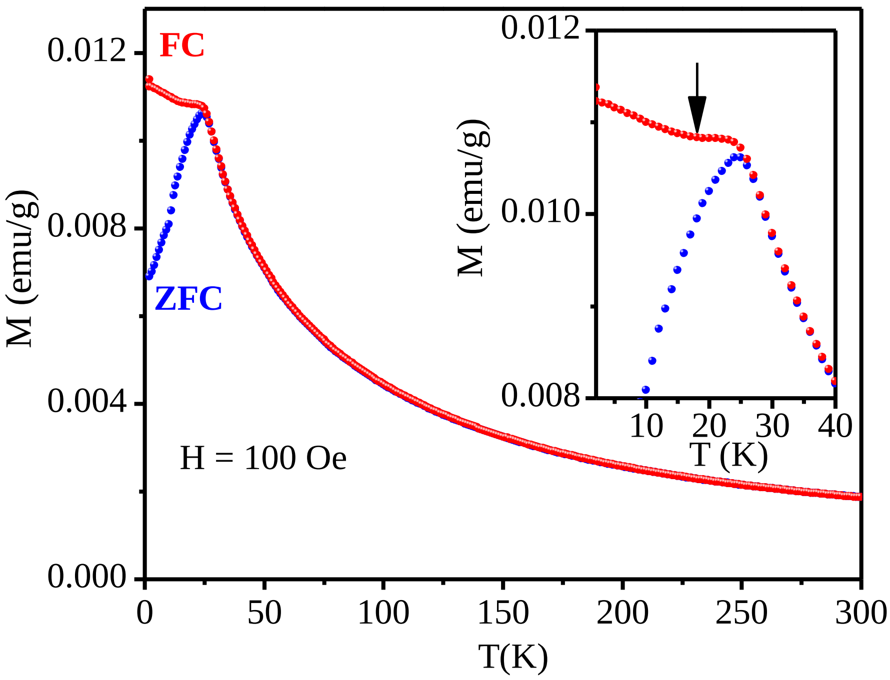

Figure 5.4: Temperature dependence of dc magnetization of $Ca(Fe_{1/2}Nb_{1/2})O_3$ measured at 100 Oe field in warming cycle for both zero-field cooled (ZFC) and field cooled (FC) conditions. The inset gives a magnified view of the M(T) to reveal a small dip (marked with an arrow) in the FC M(T) below T_f.

dynamics at T_{irr} [198]. The FC M(T) curve for non-interacting SPM systems is known to increase continuously below T_B, whereas in our case the FC M(T) curve shows a small dip just below the peak temperature over a narrow temperature range before it begins to rise again. Such a behaviour is known to occur in cluster spin-glass (CSG) systems with interacting spin clusters [198].

5.4.4 Evidence for critical slowing down of the spin dynamics: AC susceptibility studies:

The analysis of the dc magnetisation data presented in the previous section suggests the existence of SG freezing with T_f ~25K. In order to rule out the possibility of SPM blocking leading to the peak in ZFC dc M(T) and bifurcation of ZFC and FC M(T), we carried out a study of the spin/cluster dynamics using frequency and temperature dependent ac magnetic susceptibility ($\chi(\omega, T)$) measurements. Fig. 5.5(a) depicts the variation of the real ($\chi'(\omega, T)$) part of ac susceptibility of CFN measured at various frequencies for an applied ac drive field of 1 Oe. It is evident from the figure that the temperature corresponding to the peak in the $\chi'(\omega, T)$) plot shifts to higher temperatures side with increasing frequency. Although a frequency dependent shift of $T_f(\omega)$ is known for both SG freezing and SPM blocking [24,41–43,198], a distinction between the two can be made using the empirical Mydosh parameter (*K*) [42] discussed in chapter III:

$$K=\frac{1}{T_f(\omega)}\frac{\Delta T_f(\omega)}{\Delta(\ln\omega)} \qquad \text{...........} \; (5.1)$$

where $\Delta T_f(\omega)$ is the difference between the peak temperatures of $\chi'(\omega, T)$ at low and high frequencies. For SG/CSG freezing, the Mydosh parameter lies in the range 0.005-0.09 whereas it usually lies in the 0.1 to 0.3 range for SPM blocking [24,42]. In the present case, the Mydosh parameter comes out to be 0.045 which suggests that the frequency dispersion of $T_f(\omega)$ is due to SG/CSG freezing and not SPM blocking.

As discussed in chapter III, the frequency dependence of the SG freezing temperature ($T_f(\omega)$) in the scaling theories of spin-glasses has been modelled using a power law behaviour which predicts critical-slowing down of the spin dynamics and its divergence at T_{SG} at which the ergodic symmetry is broken [261]:

$$\tau = \tau_0\left(\frac{T_f(\omega) - T_{SG}}{T_{SG}}\right)^{-z\nu} \qquad \text{........} (5.2)$$

Here, τ_0 the inverse of the attempt frequency (i.e. attempt time), T_{SG} the SG transition temperature at which τ diverges, ν the critical exponent of the correlation length $\xi = (T_f/T_{SG}-1)^{-\nu}$ and z the dynamic exponent $\tau \sim \xi^z$. The relaxation time τ corresponding to the peak temperature $T_f(\omega)$ for each measuring frequency $\omega=2\pi f$ was determined using $\tau =$

1/2πf. A least-square fit to the ln(τ) versus ln(T_f/T_{SG}-1) plot shown with solid line in Fig. 5.5(b) gives T_{SG} = (23.9 ± 0.4) K, $\tau_0 = 1.47\text{x}10^{-6}$ s and zν = (2.01 ± 0.04). The large value of τ_0 reveals slow dynamics as expected for cluster spin glasses for which τ_0 typically lies in the range ~10^{-6}-10^{-10}s [24,42]. Such high τ_0 values have been reported in several CSG systems [296–298]. For canonical SG systems, like Cu:Mn, the value of τ_0 is of the order of ~10^{-13}s which is several orders of magnitude smaller than that for the cluster spin-glasses [24,42].

In order to cross-check the CSG dynamics, we modelled $T_f(\omega)$ using the Vogel-Fulcher (V-F) law also which has been used to describe the critical spin dynamics in some spin glasses [224], as discussed in chapter III:

$$\tau = \tau_0\, exp\left(\frac{E_a}{k_B(T_f(\omega) - T_{VF})}\right) \qquad \text{………..(5.3)}$$

Here, E_a is the activation energy, k_B the Boltzmann constant and T_{VF} (which is equivalent of T_{SG} in Eq. (5.2)) is called Vogel-Fulcher freezing temperature at which the spin dynamics diverges. SPM blocking dynamics, unlike the SG critical dynamics, does not show critical slowing down of the relaxation time but exhibits Arrhenius type of non-critical behaviour with T_{VF} = 0 in Eq. (5.3). The ln(τ) vs (1/T) plot for Arrhenius dynamics should obviously be linear. The non-linearity of this plot shown in the inset of Fig. 5.5(b) clearly rules out SPM blocking process to be responsible for the peak in the ZFC dc magnetization M(T) or ac susceptibility χ'(ω, T). On the otherhand, V-F law provides excellent fit as shown with continuous line through the data points in the inset. The least squares fitting parameters for V-F law are: T_{VF}= (23.3 ±0.1) K, E_a = 0.495 meV and $\tau_0 = 2.51\text{x}10^{-6}$s. The T_{SG} and τ_0 values obtained using power law and V-F law are comparable. It is worth mentioning here that the value of activation energy E_a= 0.495

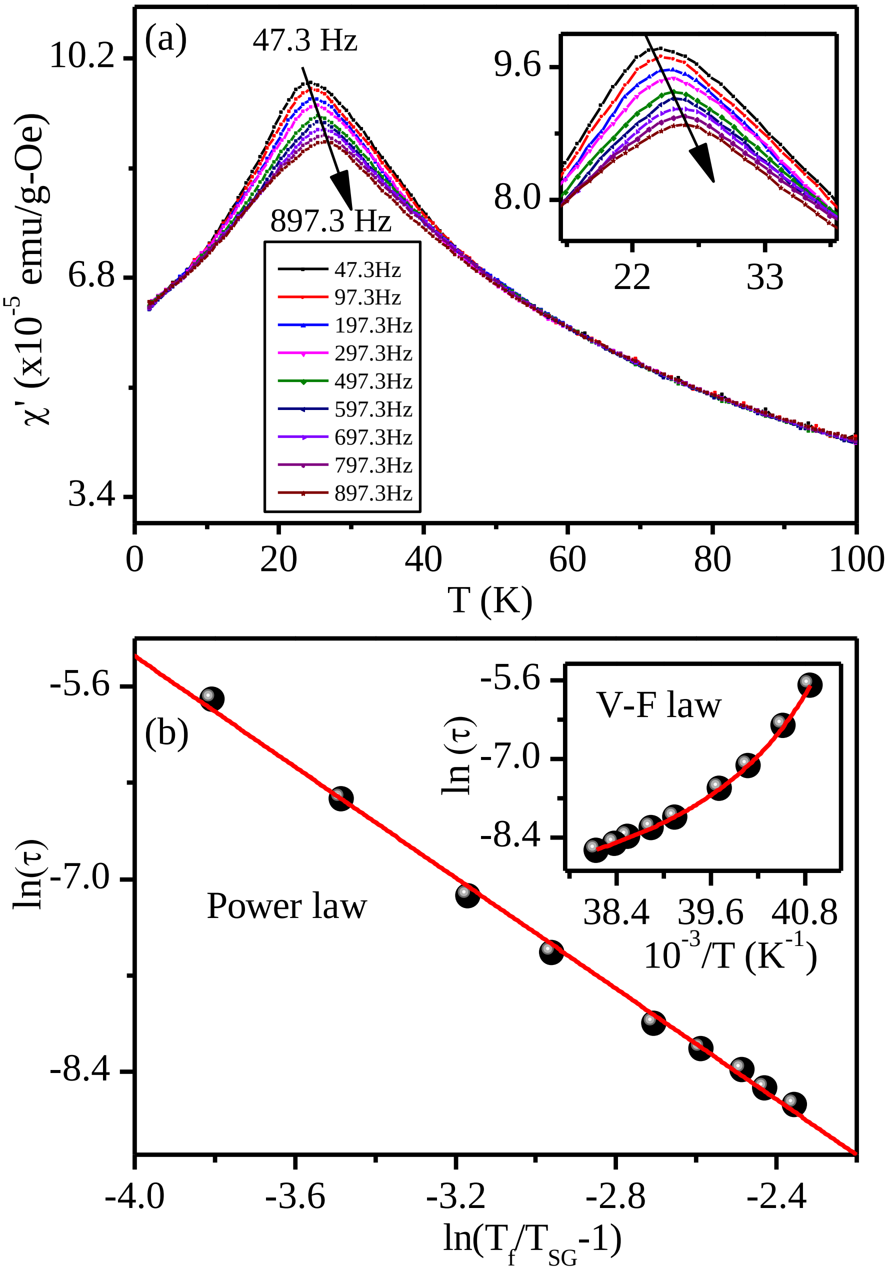

Figure 5.5: Temperature dependence of the real part ((χ' (ω, T)) of ac magnetic susceptibility of $Ca(Fe_{1/2}Nb_{1/2})O_3$ measured at various frequencies as labelled in the plot for an applied ac drive field of 1 Oe. The main panel **(b)** depict ln(τ) versus ln(T_f/T_{SG}-1) plot, where τ = 1/(2πf). Inset to panel (b) depict the ln(τ) versus 1/T plot. The solid line represents the least-squares fit for critical power law and Vogel-Fulcher law.

meV (i.e., 5.74 K) is comparable to the activation energies reported for frustrated CSG systems (e.g., $Eu_xSr_{1-x}S$) but lower than those for the canonical Ruderman-Kittel-Kasuya-

Yosida type spin glasses [224]. Thus, both the power law and Vogel-Fulcher fits confirm CSG freezing in CFN with T_{SG}~24±1 K and $\tau_0 = (2\pm0.5)\text{x}10^{-6}$s.

5.4.5 Evidence for the existence of de Almeida-Thouless line in the H-T plane:

Using the concept of replica symmetry breaking [299], it has been shown theoretically that the irreversibility temperature T_{irr}, which nearly coincides with T_f for canonical SG systems [42], would shift towards lower temperatures in the presence of magnetic field for both the Ising and Heisenberg systems [24,42]. The field dependence of T_{irr} / T_f (i.e., $T_{irr}(H)$ / $T_f(H)$) is predicted to follow the following relationship at low fields:

$$H(T) \propto \left(1 - \frac{T_f(H)}{T_f(0)}\right)^m, \qquad \ldots\ldots(5.4)$$

where the characteristic exponent m takes the value 3/2 or 1/2 for de Almeida-Thouless (A-T) [49] or Gabay-Toulouse (G-T) lines [51,52] in the H-T plane, as discussed in chapter III also. To verify the stability of the SG phase of CFN in the presence of magnetic field, we depict the ZFC and FC M(T) plots of CFN at various fields in Fig. 5.6. It is evident from the figure that the irreversibility temperature T_{irr}, marked with an arrow pointing downwards, shifts to the lower temperature side on increasing the magnetic field in agreement with the theoretical predictions [49,51,52]. Unlike CFN where the irreversibility temperature clearly observed, in the BF-0.20BT system T_{irr} is not obvious probably due to large variation in the size of the spin clusters taking part in the SG freezing process. The SG freezing temperature T_f (H), shown with an arrow pointing upwards in the same figure, corresponding to the peak in the ZFC M(T) also decreases with increasing magnetic field, similar to that observed in BF-0.20BT system. Fig. 5.7 depicts a plot of T_{irr} versus $H^{2/3}$ as well as T_f(H) versus $H^{2/3}$. It can be seen from

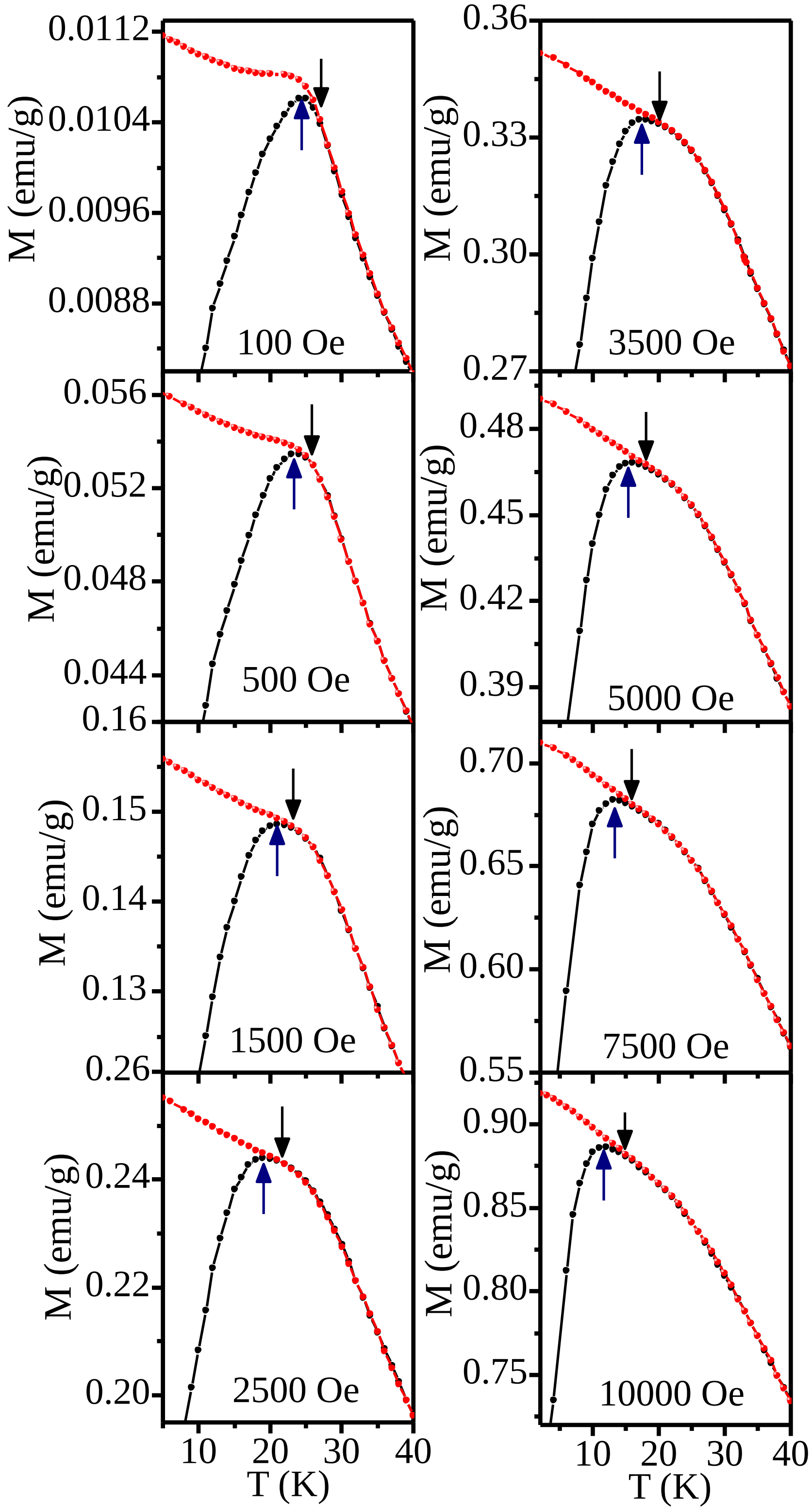

Figure 5.6: Temperature dependence of the zero-field cooled (ZFC) and field-cooled (FC) dc magnetization plots of $Ca(Fe_{1/2}Nb_{1/2})O_3$ at various applied magnetic fields. The arrow pointing downwards represents the irreversibility (T_{irr}) temperature while the arrow pointing upwards corresponds to the peak (T_f) in the ZFC M(T).

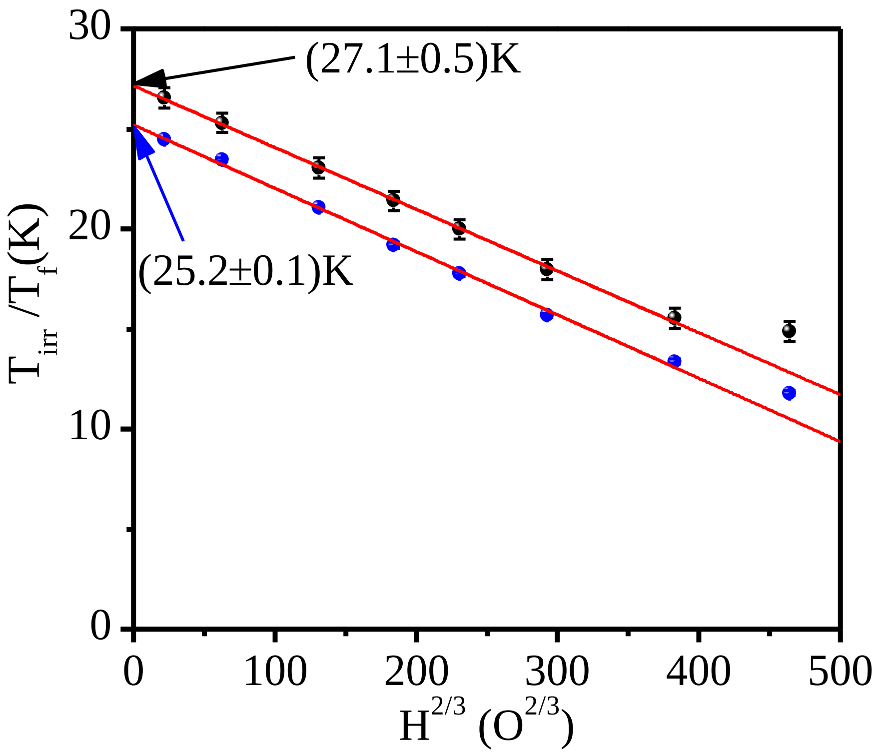

Figure 5.7: Plot of T_{irr} versus $H^{2/3}$ as well as T_f versus $H^{2/3}$ showing the presence of de Almeida-Thouless (A-T) line.

this figure that both the plots are linear below 7500 Oe confirming A-T type field dependence of T_{irr}(H) as well as T_f(H). The extrapolation of the A-T line to H = 0 gives the SG transition temperature T_{SG} ~27.1K and 25.2 K, using T_{irr}(H) and T_f(H) temperatures, respectively. The difference between T_{irr}(H) and T_f(H) at each field is about 2K which is also reflected in the T_{SG} temperature obtained from these two characteristic temperatures. We note that the value of T_{SG}~25.2K obtained from T_f(H) versus $H^{2/3}$ plot is closer to that obtained from power law/Vogel-Fulcher spin dynamics.

The A-T line has been reported for both the canonical SG as well as CSG systems using field dependence of either T_{irr}(H) [300–302] or T_f(H) [303–305] and represents the boundary between the high temperature ergodic and low temperature non-ergodic phases. While the original formulation for the A-T line was for Ising spins [49], subsequent theoretical papers have shown that it can occur in Heisenberg systems also if the single ion anisotropy is low and positive [52]. It is therefore not possible to comment on the nature of the spins (Ising versus Heisenberg) in CFN on the basis of Fig. 5.7.

5.4.6 Other characteristic features of the spin-glass phase of CFN:

Having confirmed the existence of CSG freezing with T_f ~25K in CFN, we now proceed to examine the characteristic properties of glassy state, namely slow relaxation of the thermoremanent magnetization [24,42,262], memory and rejuvenation effects [198]. The slow relaxation of thermoremanent magnetization (TRM) below T_{SG} in SG and CSG systems has been a subject matter of theoretical and experimental investigations by several workers [171,262,300]. Palmer et al. [262] have presented a generalised theory for strongly interacting SG systems, including spin clusters, in terms of a hierarchically constrained dynamics and have shown that the time dependence of TRM should exhibit a stretched exponential behaviour [171]:

$$M(t)=M_0\exp[-(t/\tau)^{\beta}] \qquad \text{….(5.5)}$$

where M_0 is the initial magnetization at $t = 0$, τ the characteristic relaxation time and β the exponent for the stretched exponential function. The value of β usually lies between 0 and 1 for different class of SG systems [24,42,198]. In this context, β =1 means, the system has monodispersive Debye like relaxation while β =0 implies absence of any relaxation. The intermediate values of β in the range $0< \beta <1$ implies a non-Debye behaviour with distribution of relaxation times due to the presence of a large number of degenerate states in the frozen state. We investigated the slow relaxation of the TRM in the glassy phase of CFN using the stretched exponential function given by Eq. (5.5). For this, the sample was first cooled in an applied magnetic field of 1000 Oe from 300 K to 15 K (i.e., below the SG freezing temperature T_f) and then allowed to age for a wait time $t_w = 10^3$s with field applied. After the waiting time, the field was switched off to zero and magnetization was measured as a function of time for 10^4s. The results are shown in Fig. 5.8 where the continuous line shows the best fit to the stretched exponential function of Eq. (5.5) with $M_0 = 0.035$, $\tau = (40166 \pm 77)$s and $\beta = 0.10$. The value of the exponent $\beta = 0.10$ not only lies in the typical range for spin glasses and cluster spin glasses but also indicates strongly polydispersive non-Debye relaxation, characteristic of the strongly interacting glassy systems in general [171]. It is interesting to compare the relaxation behaviour of TRM of CFN with that of BF-0.20BT discussed in chapter III. In BF-0.20BT system, due to the coexistence of LRO AFM phase with SG phase a nearly time independent constant TRM value was also required besides the stretched exponential function for fitting the observed relaxation behaviour. In contrast, because there is no coexisting LRO phase in CFN, only the stretched exponential term was sufficient to account for the relaxation behaviour.

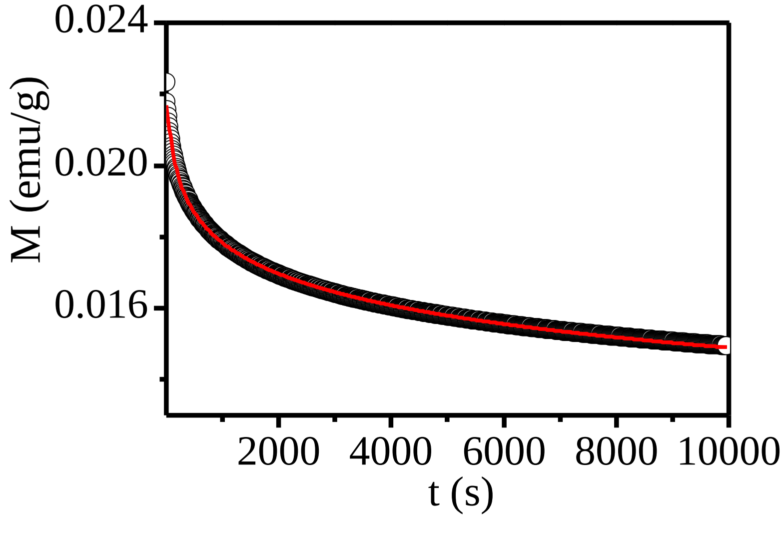

Figure 5.8: Time dependence of thermoremanent magnetization of $Ca(Fe_{1/2}Nb_{1/2})O_3$ sample at 15 K for 1000 Oe cooling field and wait time of 1000s. The solid line is the best fit for stretched exponential function to the data.

Both spin glasses and cluster spin glasses are known to exhibit aging, memory and rejuvenation effects [198,279,300,306] due to chaotic ground state of the SG phase [307]. Towards understanding the important characteristic of glassy phase, two different models have been proposed to describe the spin-glass state. In the Droplet model [308], only one spin configuration exists in the free energy landscape at a given temperature whereas in the case of Hierarchical model [309] multi-valleyed spin configurations have been postulated which split into new sub-valleys on decreasing temperature and merge on increasing the temperature. We followed three different protocols to verify the aging, memory and rejuvenation effects in the CSG phase of CFN.

In the first protocol, the sample was initially cooled under zero field (ZFC) from T = 300K which is greater than T_f to a wait temperature T_w=15K, which is less than T_f ~25K, at which the sample was allowed to age for a wait time of $t_w=10^4$s. After ageing for $t=t_w$, the sample was allowed to cool further in zero field down to 2K. After such a zero-field cooling with an intermediate wait at T_w=15K for $t_w=10^4$s, the magnetization (M_{wait}^{ZFC}(T)) was measured during the heating cycle under 100 Oe field (see Fig. 5.9(a)). This magnetization curve (M_{wait}^{ZFC}(T)) was compared with a reference curve M_{ref}^{ZFC}(T) which was obtained by measuring magnetization during heating cycle under identical field (i.e., 100 Oe) after the sample was cooled in zero field up to 2K without any intermediate stop /wait at 15K. Fig. 5.9(b) depicts the difference ΔM (T) = M_{wait}^{ZFC}(T) - M_{ref}^{ZFC}(T) vs temperature (T) plot from which it is evident that a sharp dip occurs exactly at the waiting temperature (T_w). Such a “hole burning” in the difference plot clearly demonstrates memory and rejuvenation effect in the CSG phase of CFN [198].

The second protocol involves FC condition [279]. Here, the sample was first cooled in 100 Oe magnetic field from 300 K to 2 K at a constant rate of 2K/min and then

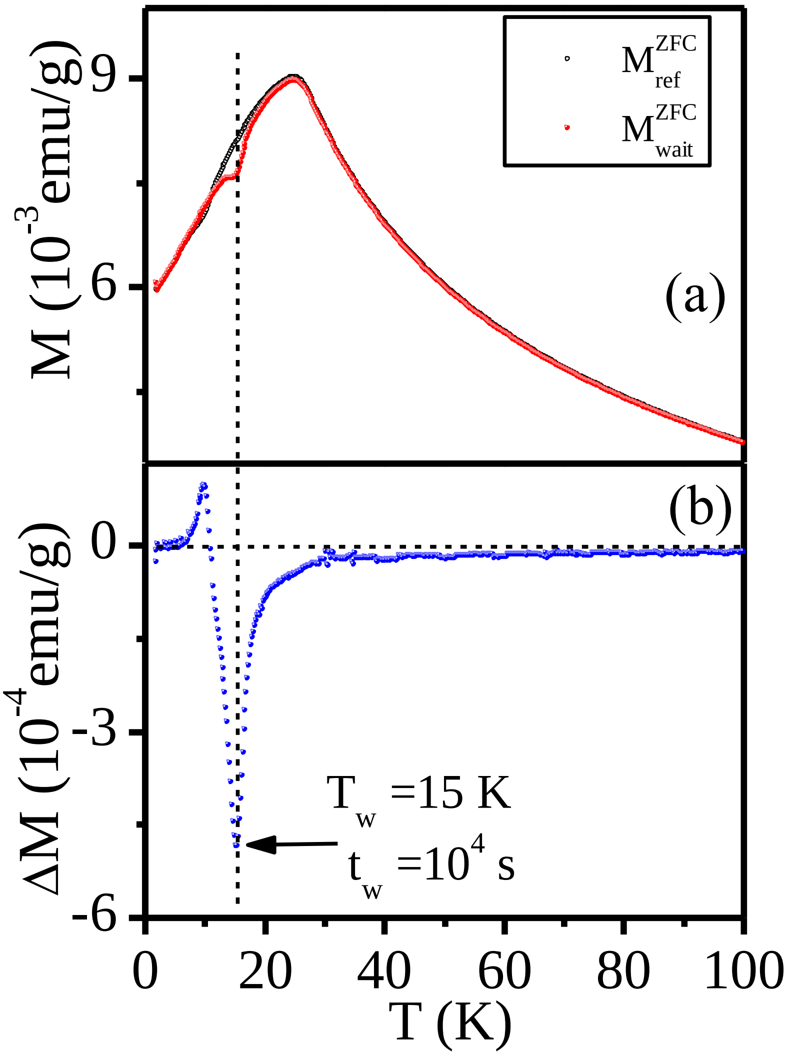

Figure 5.9: Temperature dependence ZFC magnetization of $Ca(Fe_{1/2}Nb_{1/2})O_3$ recorded at 100 Oe field with (●) and without (o) intermediate stop at T_w=15K for a wait time (t_w) of 10^4s. **(b)** depicts the difference ΔM (T) = M^{ZFC}_{wait}(T) - M^{ZFC}_{ref}(T) vs temperature (T) plot from which it is evident that a sharp dip occurs exactly at the waiting temperature (T_w).

heated back continuously at the same rate and magnetization M(T) was recorded under the same field. This gives the reference curve (M^{FCW}_{ref}(T)) shown with continuous line in Fig. 5.10. This sample was cooled again from 300K to 2K at the same rate of cooling (2K/min) and under identical field (i.e., 100 Oe) but the sample was allowed to wait at two intermediate temperatures T =50 and 15 K, which are above and below T_f, respectively, for a wait time t_w = 3 hours each. The field was set to zero during the wait time at both the temperatures. After the completion of the wait time, the field was reapplied and the measurement was resumed during further cooling. The M(T) curve so obtained is labelled as M_{wait}^{FCC}(T) and is shown with plus (+) symbol in Fig. 5.10. After cooling the sample to the lowest temperature 2K in this way, the magnetization (M_{mem}^{FCW}(T)) measurement was carried out during heating cycle maintaining the same rate (i.e., 2K/min) and the same field (i.e., 100 Oe). The results are shown with open (o) circles in Fig. 5.10. It is evident from the figure that the M_{wait}^{FCC}(T) curve shows a step at the wait temperature T_w =15K below T_f. However, no such step is observed at the other wait temperature T_w = 50K greater than T_f ~25K. Further, all the three curves merge above T_f. This protocol based on measurements done during both heating and cooling

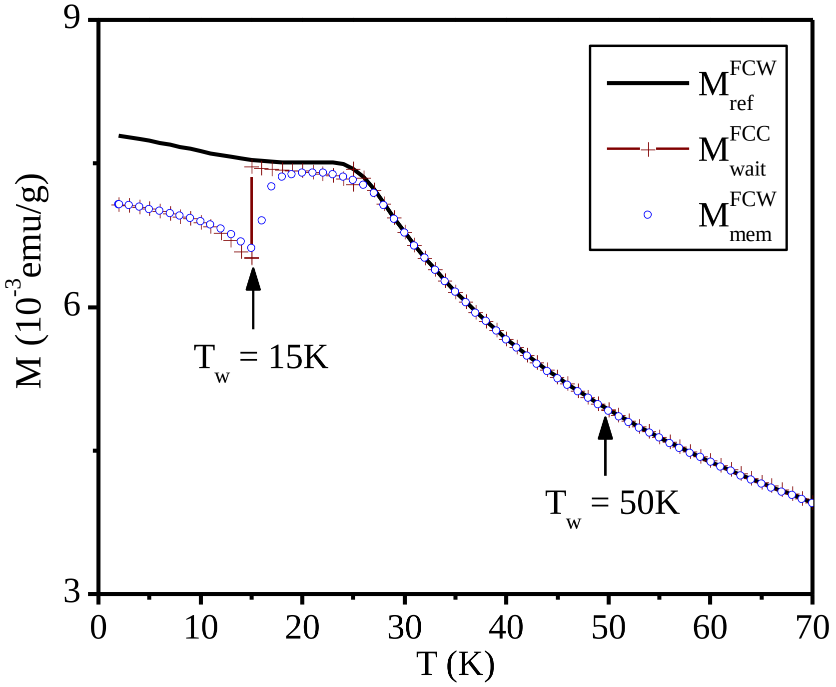

Figure 5.10: Temperature dependence dc magnetization of Ca($Fe_{1/2}Nb_{1/2}$)O_3 recorded at 100 Oe field in three different cycles as labelled in the plot. The field is set to zero during the intermittent wait of cooling temperature T_w = 50K, 15K for 3 hours. The cooling and heating rate of measurement is 2K/min. The pronounced steps in the cooling curve occurs at 15K and no such step is seen above the spin-glass freezing temperature (i.e. at 50K).

cycles further confirm that the sample remembers the measurement history. The observation of memory and rejuvenation effect rules out SPM blocking and confirms the existence of the glassy phase below T_f ~25K.

We followed a third protocol proposed by Sun et al. [279] for memory effect as this protocol enables to make a distinction between the Droplet [308] and Hierarchical [309] models of the spin glass state. As per the ZFC protocol, sample was first cooled under zero magnetic field from 300K to 15K at the rate of 2K/min and then the growth of M(t) was recorded on application of a 100 Oe field from time t=0 to $t=t_1$ =4000s (see Figs. 5.11(a)). After time $t=t_1$, the sample was quenched down to 10K and the growth of magnetization was measured again for the time $t=t_2$ =4000s as shown in the same figure. Finally, the sample temperature was raised to 15K quickly under the same field (i.e. 100 Oe) and the growth of magnetization was recorded for time $t=t_3$ = 4000s at 15K which is also shown in Fig. 5.11(a). It is evident from this figure that the M(t) curve measured during time $t=t_3$ is a continuance of the same curve measured during the time $t=t_1$ which is shown more clearly in the inset of the same panel. This protocol clearly suggests that when sample is cycled back to 15K, i.e. the initial temperature, the state of the system is recovered. For the FC condition, the sample was cooled down from 300 to 15 K under 100 Oe magnetic field at the rate 2K/min. Immediately the field was set to zero and magnetization was measured for the time $t=t_1$=4000s. After the elapse of time t $=t_1$, the sample was quenched down to 10K (here the field was still zero) and the evolution of magnetization M (t) was measured for the time $t=t_2$ = 4000s. Finally, the sample was heated back again to 15K and the evolution of magnetization was recorded for time $t=t_3$=4000s. It is evident from panel (b) of Fig. 5.11 that the state of the system is recovered when the temperature returns to initial 15K. Further, the relaxation of magnetization M(t) curve during the time t_3 is a continuance of $t = t_1$ as shown more

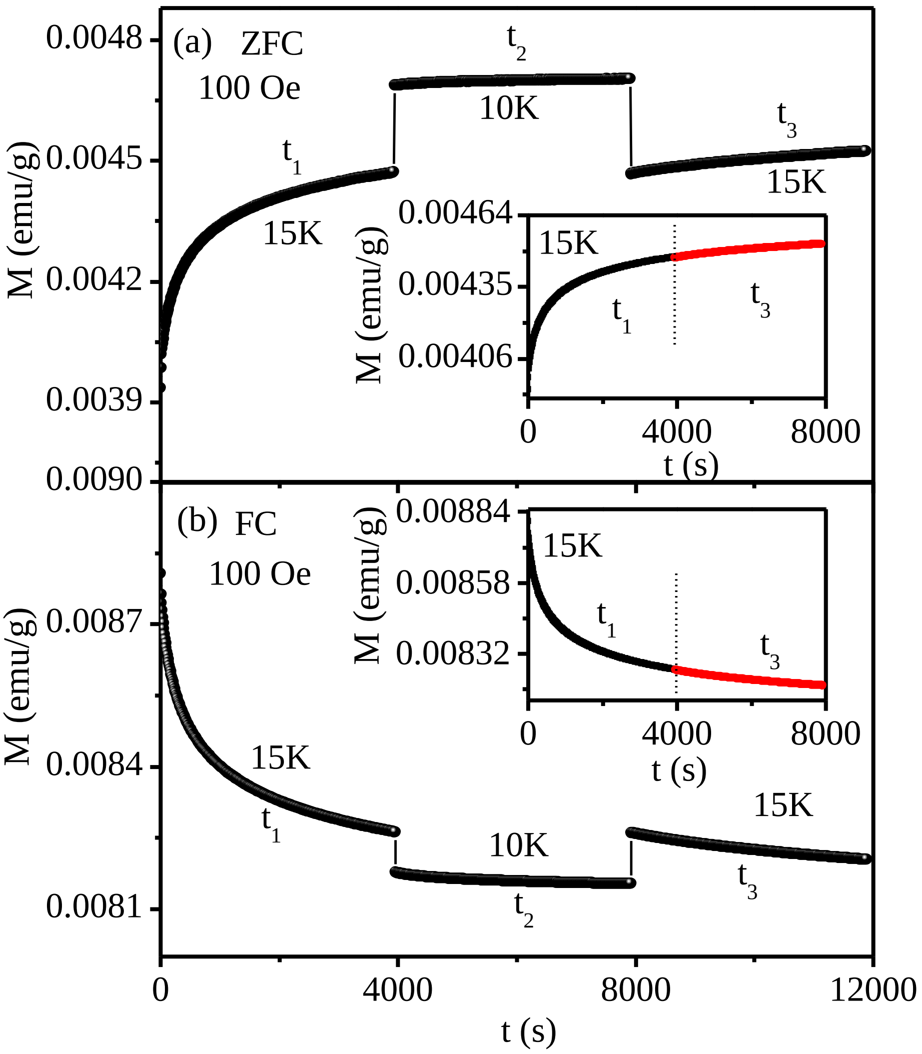

Figure 5.11: Magnetic relaxation of $CaFe_{1/2}Nb_{1/2}O_3$ sample at 15 K for 100 Oe field with temporary cooling (i.e. negative cycling) at 10K using (a) the ZFC and (b) FC protocols. The insets show the same data versus total time spent at 15K. The relaxation curve clearly reveals that, the curve during t_3 is in continuation of the curve during t_1 (memory effect).

clearly in the inset of the same panel. Our observed relaxation behaviour can be explained in the context of Hierarchical model of SG system. At a given temperature say T_0 =15K, several multi-valleyed states are organized in the free-energy landscape as per this model. When the sample is quenched down from T_0 =15K to T_0-ΔT =10K, then each valley is expected to split into new sub valleys as per the Hierarchical model. However, if ΔT is very large, the relaxation occurs only between the newly born sub-valley of each set. When the sample was heated back to T_0 =15K, the new born sub valleys merge back to

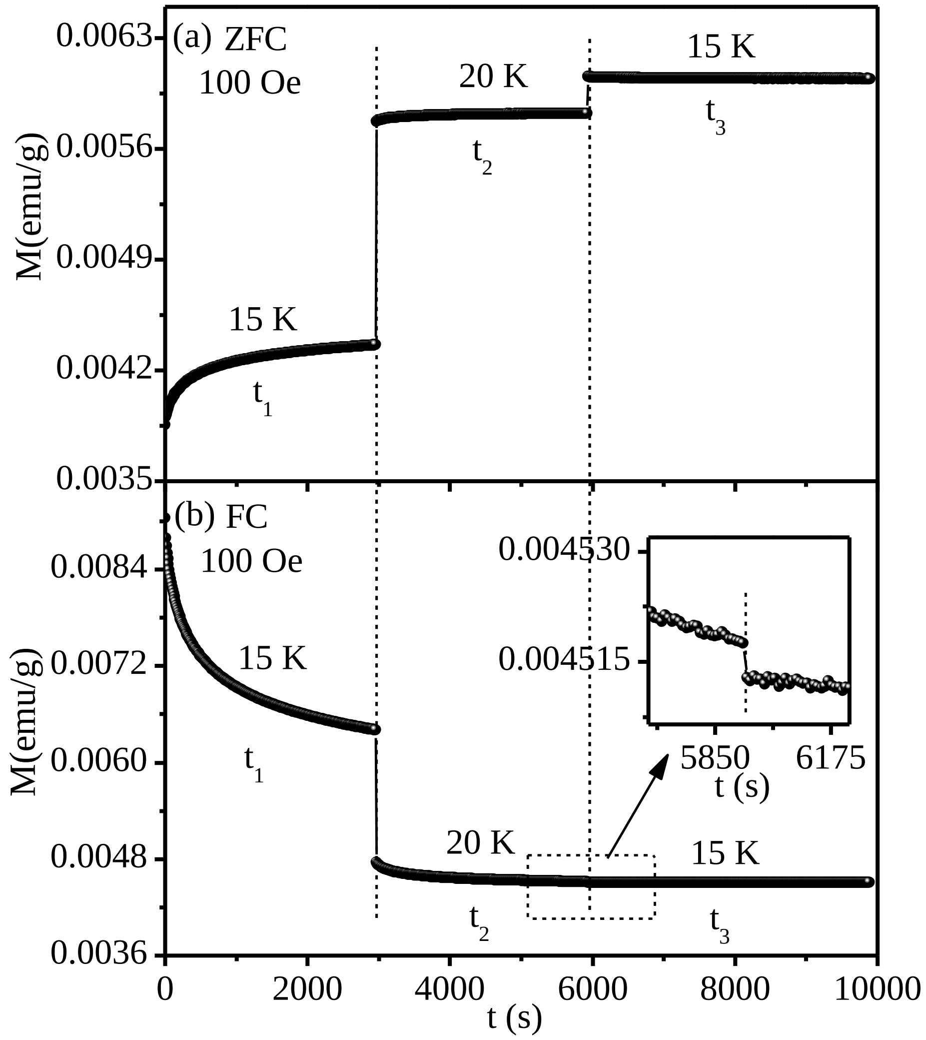

Figure 5.12: Magnetic relaxation of $CaFe_{1/2}Nb_{1/2}O_3$ sample at 15K for 100 Oe field with temporary heating (i.e. positive cycling) at 20K using (a) the ZFC and (b) FC protocols. The relaxation curve clearly reveals that during heating cycle the curve during t_3 is not in continuation of the curve during t_1 which is consistent Hierarchical model.

reproduce the initial free-energy landscape. In this way, one can explains the above observed memory and rejuvenation effect of temporary cooling cycle using the Hierarchical model. Further, we have also checked the positive temperature cycling effect on the time dependence of magnetic relaxation M(t) of CFN sample [279]. Figs. 5.12(a) and (b) display the time dependence of relaxation of CFN sample below T_{SG} under ZFC and FC conditions, respectively with positive temperature cycling. It is clearly seen from the figures that no memory effect is observed for positive temperature cycling consistent with the Hierarchical model of SG. In the Droplet model, one expects a symmetric behaviour corresponding to negative or positive cycling of temperature while in Hierarchical model, an asymmetric behaviour is expected. Thus, our results about the memory and rejuvenation effect under both ZFC and FC protocols with temperature cycling support the Hierarchical model of spin glass state.

5.4.7 Direct evidence for the presence of spin clusters in CFN using neutron diffraction:

As mentioned in section 5.4.2 the small dip in FC M(T) plot just below the SG freezing temperature T_f in the ZFC M(T) plot points towards the possibility of a CSG phase [198]. Similarly, the large value of attempt time τ_0 (~10^{-6}s), obtained from power law and V-F law fits to the temperature dependence of the spin relaxation time, also suggests that the SG phase of CFN may be of CSG type [24,42]. Neutron scattering technique can provide evidence not only for the presence of LRO AFM structure but also for short-range ordered (SRO) AFM clusters of spins in the CSG systems. The presence of SRO AFM spin clusters gives rise to diffuse scattering in the neutron scattering patterns [173,296,310–314]. Accordingly, we carried out neutron powder diffraction (NPD) measurements on powder samples of CFN to obtain direct evidence for the presence of AFM spin clusters. Fig. 5.13(a) depicts the NPD patterns of CFN at three selected temperatures, 300K, 100K and 5K, over a limited 2θ range from 5 to 90 deg. For LRO AFM phase, one expects a sharp magnetic peak corresponding to the pseudocubic Q=½½½ position shown with an arrow in Fig. 5.13(a). It can be clearly seen from this figure that no sharp magnetic Bragg peak characteristic of LRO AFM phase is observed in the NPD patterns of CFN down to 5K in marked contrast to PFN where such a peak has been observed below T_N~150K [172]. Instead, a broad diffuse peak, whose peak

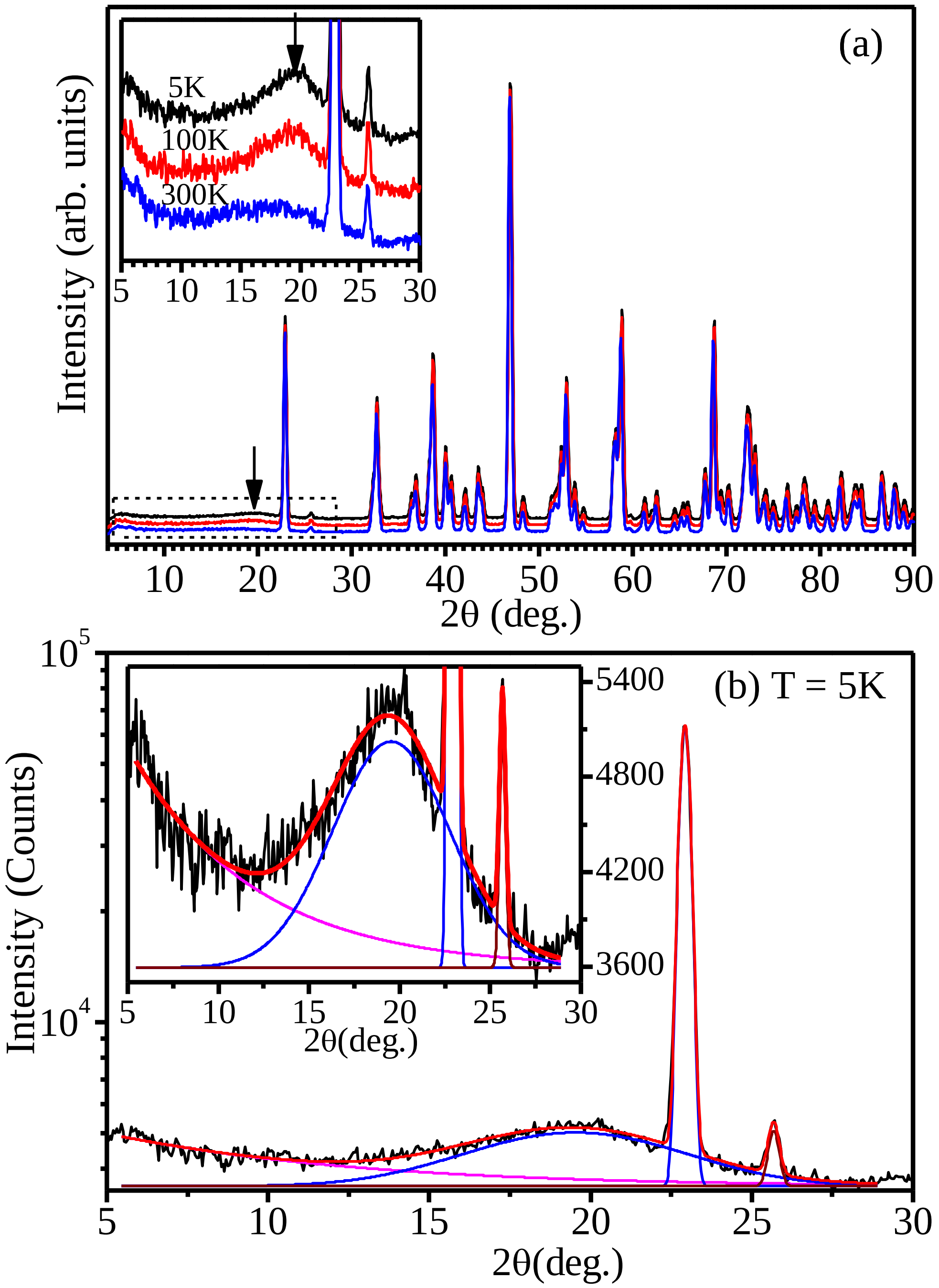

Figure 5.13: Panel **(a)** depicts neutron powder diffraction patterns of $Ca(Fe_{1/2}Nb_{1/2})O_3$ collected at 300K, 100K and 5K. The patterns are shifted vertically for the purpose of presentation. Inset of (**a**) depicts the enlarged scale of broad diffuse magnetic scattering peak corresponding to short-range antiferromagnetic correlations. Panel **(b)** depicts the deconvolution of the NPD profile peaks at 5K. Insets of panel (**b**) shows enlarged scale of deconvoluted peaks at 5K.

intensity is about 4% of the strongest nuclear peak, centred at the expected position of AFM LRO peak is clearly seen in Fig. 5.13(a) (see inset also). The observation of broad diffuse peak provides direct evidence for the presence of SRO AFM spin clusters. A similar broad diffuse peak has been reported in geometrically frustrated pyrochlores [310,311], spin-chain compounds [312,313], and spinels [314] showing CSG freezing.

It is interesting to note from Fig. 5.13(a) that the broad peak due to the short-range AFM correlated spin clusters are present even at room temperature which is much higher than T_f ~25K. It is also evident from the figure that with decreasing temperature, the intensity of the broad diffuse peak increases. In order to determine the correlation length for AFM spin clusters from the magnetic diffuse scattering, we deconvoluted the diffuse peak and the two neighbouring stronger peaks using three Gaussians and the result of the peak deconvolution is shown in Fig. 5.13(b) at 5K. The deconvoluted diffuse magnetic peak centered at $2\theta = 19.7^o$ at 5K is shown in the inset of Fig. 5.13(b). It is possible to determine the correlation length (ξ) from the FWHM of the deconvoluted diffuse magnetic peak using Scherrer formula $\xi = 0.9\lambda/\beta\cos\theta$ (Å), after removing the instrumental broadening from the observed FWHM of the diffuse peak (β_{obs}). We use the relationship $\beta = \sqrt{\beta_{\text{obs}}^2 - \beta_{\text{inst}}^2}$, where β is the intrinsic FWHM and β_{ins} is the FWHM of the instrumental resolution function to obtain the intrinsic broadening of the diffuse peak. The correlation length for the SRO spin clusters obtained from the intrinsic FWHM are (22±1), (19±1) and (14±2) Å at 5K, 100K and 300K, respectively. Thus our neutron scattering studies reveal that the size of the AFM correlated spin clusters increases slightly on lowering the temperature, but the AFM correlations could not develop to long length scales presumably due to the frustrated nature of the superexchange interactions in CFN. Our neutron scattering studies thus provide direct microscopic evidence for the presence of SRO AFM correlated spin clusters of ~2nm average size for CSG freezing in CFN.

5.5. Conclusions:

In summary, we have synthesized phase pure $Ca(Fe_{1/2}Nb_{1/2})O_3$ (CFN) by conventional solid state route and characterised it its phase purity, crystal structure, microstructure and composition using the techniques discussed in chapter II and III.

We have investigated the low temperature magnetic transition in CFN using M(T), χ (ω, T), M(T, H), M(T, t) and neutron scattering measurements. The analysis of dc magnetization measurements reveals a spin-glass (SG) phase with T_f ~25K with characteristic history dependent irreversibility. Analysis of the ac susceptibility measurements reveals power law/Vogel-Fulcher type critical spin dynamics with a time scale of τ_0~10^{-6}s which suggests the existence of a cluster spin-glass (CSG) phase in CFN below T_{SG}~24K. The field dependence of the irreversibility temperature T_{irr} (H) and the peak temperature T_f(H) of the ZFC M(T) falls on de Almeida-Thouless (A-T) line in the T_{irr}(H)/T_f (H) versus $H^{2/3}$ plot. The zero-field SG freezing temperature $T_f(0) = 25.2$K, obtained from the extrapolation of T_f(H) versus $H^{2/3}$ plot to H = 0, is in close agreement with the ergodicity breaking temperature T_{SG}~24K obtained from the analysis of the ac susceptibility $\chi(\omega, T)$ data. The observation of slow relaxation of thermoremanent magnetization, memory and rejuvenation effects below the SG transition temperature T_{SG}~24K supports glassy phase. Neutron diffraction study confirms the absence of any long-range AFM ordering but shows diffuse scattering due to the presence of short-range ordered (SRO) AFM spin clusters with a correlation length ξ ~2nm involved in the CSG freezing.